were used for the mass spectrometric analyses without further purification. The introduction of the second label in **5b** apparently has to be explained by the intermediacy of an S,S biradical.[17]

All mass spectrometric experiments were carried out in a commercially available VG Instruments ZAB-2F mass spectrometer which is of BE configuration (B stands for magnetic and E for electric sector), with standard tandem mass spectrometry conditions (see text).

(17) Egsgaard, H.; Carlsen, L. Unpublished results.

Acknowledgment. We gratefully appreciate the support of our work by the Fonds der Chemischen Industrie, Deutsche Forschungsgemeinschaft, Graduiertenkolleg Chemie, and the Gesellschaft von Freunden der Technischen Universität Berlin.

Calculation of Excited-State Geometries via the Time-Dependent Theory of Resonance Raman Spectroscopy: Application to the Complexes $Cs_4[W_2OCl_{10}]$ and $Cs_3[Re_2OCl_{10}]$

Kyeong-Sook Kim Shin,[1a] Robin J. H. Clark,*[1b] and Jeffrey I. Zink*[1a]

Contribution from the Department of Chemistry and Biochemistry, University of California, Los Angeles, California 90024, and the Christopher Ingold Laboratories, University College London, 20 Gordon Street, London WC1H 0AJ, England. *Received August 4, 1989*

Abstract: The calculation of both the excitation profiles of the resonance-enhanced Raman bands and the intensities of the overtone and combination bands of the rich resonance Raman spectra of $Cs_3[Re_2OCl_{10}]$ and $Cs_4[W_2OCl_{10}]$ is reported. The calculation uses the time-dependent theory of Lee, Tannor, and Heller. The geometric changes attendant upon excitation of each molecule from the ground to the excited state in resonance are calculated. All of the excitation profiles and the resonance Raman spectra can be fitted by use of one multidimensional potential surface.

The geometrical changes that a molecule undergoes when it is electronically excited are important in determining its spectroscopic and photochemical properties. Transition-metal complexes are of particular interest because they frequently undergo large displacements along many normal modes when excited. The magnitudes of the displacements can be calculated from the intensities of vibronic bands in electronic emission or absorption spectra if band structure can be observed.[2-6] More commonly, however, only broad unstructured bands are obtained from big transition-metal complexes in condensed media. An alternative method of calculating the displacements uses the intensities in resonance Raman spectra.[7-13] This method is especially powerful for large inorganic molecules in condensed media because most of the displaced modes can be individually observed and calculated even when only a broad envelope is observed in the electronic spectrum. The new time-dependent theory developed by Lee, Tannor, and Heller is especially efficient.[14-17]

The high polarizability of the axial π-bond system of $[M_2OX_{10}]^{n-}$ ions (M = Ru, Re, Os, or W; X = Cl or (in some cases) Br) is well-known to make them ideal species for Raman studies.[18-20] The $[Ru_2OCl_{10}]^{4-}$ ion was established from early crystallographic work to be linear, with D_{4h} symmetry,[21] and many other such ions are known to have this structure.[19] Raman studies using excitation lines at resonance with the lowest allowed electronic transition of the $[Re_2OCl_{10}]^{3-}$ ion (the $e_u^* \leftarrow e_g$, $^4E_g \leftarrow {}^4E_u$ transition of the linear Re–O–Re π-bonded system[19]) gives rise to long (up to 12-membered) overtone progressions in the $\nu_1(a_{1g})$, ν_s(ReORe), symmetric Re–O–Re stretching fundamental at 230 cm^{-1}. At least eight progressions in ν_1 are observed in the resonance Raman spectrum of this ion; in most cases, the enabling modes for the $\nu_n + \nu_1\nu_1$ progressions are other Raman-active fundamentals but, in three cases, they are the first and third overtones of infrared-active (Raman inactive) fundamentals. The other isostructural ions give rise to similar resonance Raman spectra.[18-20] The observation of long progressions in a totally symmetric mode offers the opportunity of calculating the geometric changes attendant upon excitation from the ground to the resonant excited state.

In this paper, the geometric changes in the $[W_2OCl_{10}]^{4-}$ and $[Re_2OCl_{10}]^{3-}$ ions upon excitation within the contour of the band assigned to the $e_u^* \leftarrow e_g$ transition are calculated. Excitation profiles of fundamentals, overtone, and combination bands are

(1) (a) Department of Chemistry and Biochemistry, University of California, Los Angeles. (b) Christopher Ingold Laboratories, University College London.
(2) Yersin, H.; Otto, H.; Zink, J. I.; Gliemann, G. *J. Am. Chem. Soc.* **1980**, *102*, 951 and references therein.
(3) Zink, J. I. *Coord. Chem. Rev.* **1985**, *64*, 93.
(4) Zink, J. I.; Tutt, L.; Yang, Y.-Y. *Am. Chem. Soc. Sym. Ser.* **1986**, *307*, 39.
(5) Preston, D. M.; Shin, K. S.; Hollingsworth, G.; Zink, J. I. *J. Mol. Struct.* **1988**, *173*, 185.
(6) Larson, L. J.; Zink, J. I. *Inorg. Chem.* **1989**, *28*, 3519.
(7) Clark, R. J. H.; Dines, T. J.; Doherty, J. M. *Inorg. Chem.* **1985**, *24*, 2088.
(8) Clark, R. J. H.; Dines, T. J.; Wolf, M. L. *J. Chem. Soc., Faraday Trans. 2* **1982**, *78*, 679.
(9) Clark, R. J. H.; Dines, T. J.; Proud, G. P. *J. Chem. Soc., Dalton Trans.* **1983**, 2019.
(10) Clark, R. J. H.; Dines, T. J.; Kurmoo, M. *Inorg. Chem.* **1983**, *22*, 2766.
(11) Tutt, L.; Tannor, D.; Schindler, J.; Heller, E. J.; Zink, J. I. *J. Phys. Chem.* **1983**, *87*, 3017.
(12) Shin, K. S.; Clark, R. J. H.; Zink, J. I. *J. Am. Chem. Soc.* **1989**, *111*, 4244.
(13) Shin, K. S. K.; Zink, J. I. *Inorg. Chem.* **1989**, *28*, 4358.
(14) Lee, S.-Y.; Heller, E. J. *J. Chem. Phys.* **1979**, *71*, 4777.
(15) Heller, E. J. *Acc. Chem. Res.* **1981**, *14*, 368.
(16) Heller, E. J.; Sundberg, R. L.; Tannor, D. *J. Phys. Chem.* **1982**, *86*, 1822.
(17) Tannor, D.; Heller, E. J. *J. Phys. Chem.* **1982**, *77*, 202.
(18) Clark, R. J. H.; Franks, M. L.; Turtle, P. C. *J. Am. Chem. Soc.* **1977**, *99*, 2473.
(19) Campbell, J. R.; Clark, R. J. H. *Mol. Phys.* **1978**, *36*, 1133.
(20) Campbell, J. R.; Clark, R. J. H. *J. Chem. Soc., Faraday Trans. II* **1980**, *76*, 1103.
(21) Mathieson, A. M.; Mellor, D. P.; Stephenson, N. C. *Acta Crystallogr.* **1952**, *5*, 185.

0002-7863/90/1512-3754$02.50/0

calculated and compared with those derived from the experimental spectra.

Experimental Section

The details on the Raman spectra of $Cs_3[Re_2OCl_{10}]$[19] and $Cs_4[W_2OCl_{10}]$[20] have been reported elsewhere. The intensities of each resonance-enhanced band at each available excitation wavelength have been estimated from the product of the peak heights and full-widths at half-height (triangular approximation). The relative intensities of all of the peaks in the resonance Raman spectra were also estimated by use of the triangular approximation method.

Theory

The theoretical treatment of the resonance Raman data is based on the time-dependent theory of Lee and Heller.[14-17] The calculation in the time domain is very efficient because the evaluation of Frank–Condon (F–C) factors and the sum-over-states is avoided. The intensities of a large number of vibrational bands including overtone and combination bands can readily be calculated. Because the details of the theory have been presented in both the original theoretical papers[14-17] and in applications to other metal-containing molecules,[12,13] only the essential features are given here.

The Raman scattering cross section is given by[17]

$$(\alpha)_{fi} = \frac{i}{\hbar}\int \langle\phi_f|\phi(t)\rangle \exp\{(i\omega' - \Gamma)t\}\,dt \qquad (1)$$

where $|\phi_f\rangle = \mu|\chi_f\rangle$ is the final vibrational state of the ground electronic surface multiplied by the transition electric dipole moment, $|\phi(t)\rangle = \exp(-iH_{ex}t/\hbar)|\phi\rangle$ is a moving wavepacket propagated by the excited-state Hamiltonian, $|\phi\rangle = \mu|\chi\rangle$ is the initial vibrational state of the ground electronic surface multiplied by the electronic transition moment, Γ is the damping factor, $\omega' = \omega_i + \omega_1$, $\hbar\omega_i$ is the zero-point energy of the ground electronic surface, and $\hbar\omega_I$ is the energy of the incident radiation.

The resonance Raman scattering amplitude is governed by the motion of a wavepacket on a multidimensional hypersurface representing the excited electronic state potential. The initial wavepacket, ϕ, makes a vertical transition onto the potential surface of the excited state which, in general, is displaced relative to that of the ground state. The displaced wavepacket is not a stationary state and evolves according to the time-dependent Schrödinger equation. The quantity of interest is the overlap of the moving wavepacket $\phi(t)$ with the final state of interest ϕ_f. ϕ_f is the wave function of the normal mode k with vibrational quantum number n_k. If it is assumed that (a) only one electronic excited state is involved, (b) the potential surfaces are harmonic, (c) the normal coordinates are not mixed in the excited state, (d) the transition dipole moment, μ, is constant, and (e) the force constants are the same in both the ground and the excited states, then the overlap for the totally symmetric modes has the simple form

$$\langle\phi|\phi(t)\rangle_s = \prod_k \left\{\exp\left[-\frac{\Delta_k^2}{2}(1 - \exp(-i\omega_k t)) - \frac{i\omega_k t}{2}\right] \times (1 - \exp(-i\omega_k t))^{n_k}\frac{(-1)^{n_k}\Delta_k^{n_k}}{(2^{n_k}n_k!)^{1/2}}\right\} \exp(-i\omega_0 t) \qquad (2)$$

In eq 2, ω_0 is the wavenumber of the zero–zero electronic transition (E_{00}) in cm^{-1}, ω_k and Δ_k are respectively the wavenumber in cm^{-1} and the displacement of the kth normal mode, and n_k is the vibrational quantum number of the kth normal mode in the ground electronic state ($n_k = 0, 1, 2$, etc.). Equation 2 is used to calculate the cross sections for the fundamentals and all the various overtone and combination bands. For example, in order to calculate the cross section of the combination band ($\nu_2 + \nu_3$) in a three mode case, $n_1 = 0$, $n_2 = 1$, and $n_3 = 1$.

None of the approximations that are used in the derivation of eq 2 are requirements of the time-dependent theory. The harmonic approximation is used in this paper because the number of parameters to be fitted is thereby reduced and because it allows the simple expression for the overlap (eq 2) to be used. Because there is no distinct evidence of normal mode mixing in the molecules studied here, all of the fits were done without including the additional parameters of mode mixing. Assumption (e) introduces at most an error of 10% if the distortions are very large.[2] When the vibrational frequencies in the excited state are not known, this assumption must be used but does not introduce serious error. These assumptions are good for many systems and are valid for the examples reported here.

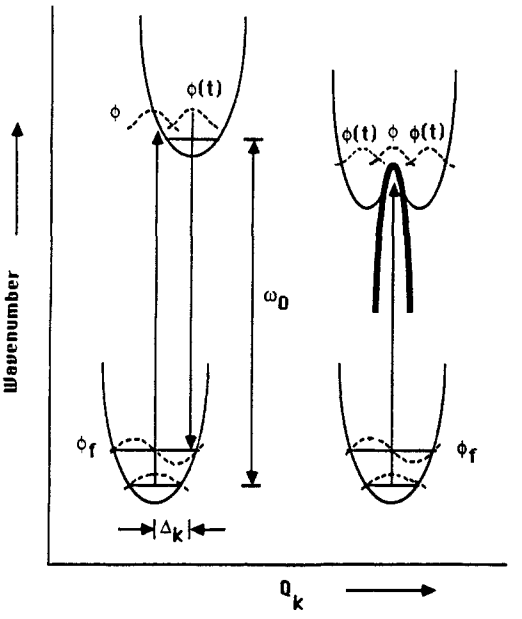

Figure 1. Illustration of the time-dependent theory of resonance Raman scattering for a totally symmetric mode (left) and for a non-totally symmetric mode (right). ϕ is the initial wavepacket, $\phi(t)$ is the moving wavepacket, ϕ_f is the final state of interest, and Δ_k is the displacement of the upper potential surface along the normal coordinate Q_k.

The calculation of the resonance Raman scattering amplitude for a non-totally symmetric mode presents a more complicated problem. A simple model that will be used here to describe the potential surface in the excited state along the non-totally symmetric mode is the inverted harmonic oscillator. This surface is used to model the actual potential surface in the region of the ground-state internuclear geometry as shown on the right in Figure 1. This simple model has a zero slope at the internuclear geometry and decreases in energy in both directions along the normal coordinate as is required for a non-totally symmetric mode. This simple model will break down at large Δ's because the surface is unbound. However, if Γ is sufficiently large, the wavepacket will only explore the immediate vicinity of the F–C region and the inverted surface is a good approximation. The initial wavepacket, ϕ, makes a vertical transition to the potential surface on the excited state. The wavepacket propagates on the surface by spreading on the parabolic barrier because it is not an eigenfunction of the surface and the slope of the surface of a non-totally symmetric mode and of the inverted harmonic oscillator surface is zero at the equilibrium internuclear position of the ground state.

The overlap for non-totally symmetric modes, $\langle\phi_f|\phi(t)\rangle_{ns}$, on such a surface has been derived by Kinsey et al.[22]

$$\langle\phi_f|\phi(t)\rangle_{ns} = \prod_j \left\{\frac{\sqrt{n_j!}}{2^{n_j}(n_j/2)!}\left(c_j + \frac{i}{2}s_j\left(\frac{\omega_j}{\omega_j'} - \frac{\omega_j'}{\omega_j}\right)\right)^{-1/2} \times \left(\frac{is_j\left(\frac{\omega_j}{\omega_j'} + \frac{\omega_j'}{\omega_j}\right)}{c_j + \frac{i}{2}s_j\left(\frac{\omega_j}{\omega_j'} - \frac{\omega_j'}{\omega_j}\right)}\right)^{n_j/2}\right\} \qquad (3)$$

(22) Johnson, B. R.; Kinsey, J. L. *J. Chem. Phys.* **1987**, *87*(3), 1525.

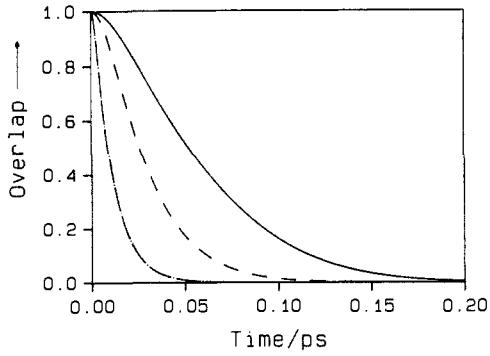

Figure 2. The magnitude of damped overlap for $f = 0$, $|\langle\phi_f|\phi(t)\rangle_{ns} \exp(-\Gamma t)|$, versus time. $\omega_j = 370.7$ cm^{-1}, $\omega_j' = 100$ cm^{-1} (—), 400 cm^{-1} (---), and 1000 cm^{-1} (-·-), and $\Gamma = 50$ cm^{-1}.

In equation 3, ω_j is the wavenumber of a non-totally symmetric mode in the ground state in cm^{-1}, ω_j' is the wavenumber of the inverted harmonic surface in the excited state in cm^{-1}, c_j is equal to cosh $(\omega_j' t)$ and s_j is equal to sinh$(\omega_j' t)$, and n_j is the vibrational quantum number of the jth non-totally symmetric normal mode in the ground electronic state ($n_j = 0, 1, 2$, etc.).

Figure 2 shows a plot of the magnitude of the overlap for $f = 0$, $|\langle\phi_f|\phi(t)\rangle_{ns}|$, versus time. The magnitude of the overlap decreases as the wavepacket spreads out. There is no recurrence. The steeper the inverted potential (i.e. the higher ω_j'), the faster the wavepacket spreads out and the faster the overlap decreases. Because the inverted harmonic potential surface can model only a small area around the Frank–Condon region, this model can only be applied to short-time dynamics.

The total overlap is the product of the overlap of totally symmetric modes ($\langle\phi_f|\phi(t)\rangle_s$) and that of the non-totally symmetric modes ($\langle\phi_f|\phi(t)\rangle_{ns}$).

$$\langle\phi_f|\phi(t)\rangle = \langle\phi_f|\phi(t)\rangle_s \times \langle\phi_f|\phi(t)\rangle_{ns} \quad (4)$$

The Raman scattering amplitude in the frequency domain is the half-Fourier transform of the overlap in the time domain as shown in eq 1. The Raman intensity $I_{i\to f}$ into a particular mode f is

$$I_{i\to f} \equiv \omega_l \omega_s^3 [\alpha_{fi}]^* [\alpha_{fi}] \quad (5)$$

where ω_s is the wavenumber of the scattered radiation.

Application of the Theory to $Cs_3[Re_2OCl_{10}]$ and $Cs_4[W_2OCl_{10}]$

Calculation of the Excitation Profiles and Resonance Raman Spectra. The resonance Raman spectra and the excitation profiles of $Cs_3[Re_2OCl_{10}]$ and $Cs_4[W_2OCl_{10}]$ are calculated from a given set of values for Δ_k, ω_k, ω_j, ω_j', ω_l, Γ, and E_{00} by use of eq 1 through 4. E_{00} is estimated from the electronic absorption spectrum and the ω_k's and ω_j's are determined from the Raman and infrared spectra. ω_l is the excitation wavenumber used to obtain the resonance Raman spectrum. The variable parameters are Δ_k and Γ and the parameter governing the steepness of the inverted potential is ω_j'. Only one set of parameters is used for each complex to calculate all of the excitation profiles for the fundamental, overtone, and combination bands, to calculate the resonance Raman spectrum at a given excitation wavelength, and to calculate the absorption spectrum.

$Cs_4[W_2OCl_{10}]$. The excitation profiles of best fit for the fundamental ν_1, ν(W–O–W), and overtones $2\nu_1$ and $2\nu_9$ (the first overtone band of δ(W–O–W)) are shown in Figure 3. They are calculated by use of the parameters given in Table I. The calculated and experimental excitation profiles (Figure 3) are in good agreement. The band widths and shapes of each excitation profile and relative intensities are accurately calculated. The calculated maxima of the excitation profiles lie at ~18 500 cm^{-1}, about 400 cm^{-1} higher than the maximum of the electronic absorption band (~18 100 cm^{-1}) with which the specified laser line is in resonance.

The absorption spectrum can also be calculated by using the same parameters that were used to calculate the excitation profiles.

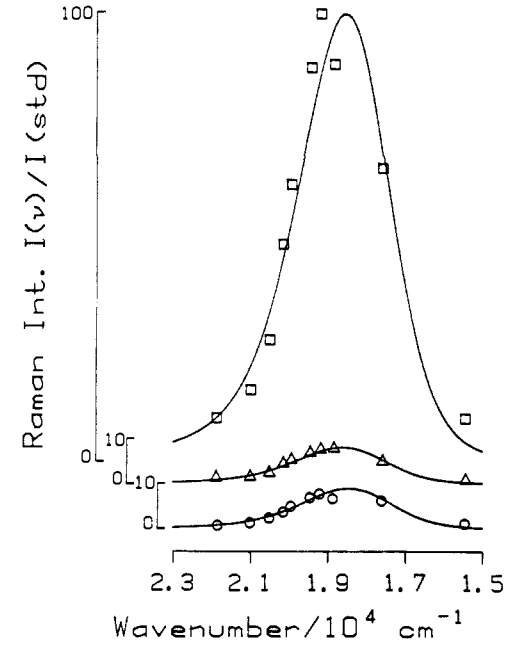

Figure 3. Calculated and experimental resonance Raman excitation profiles of ν_1 (□), $2\nu_1$ (△), and $2\nu_9$ (○) for $Cs_4[W_2OCl_{10}]$.

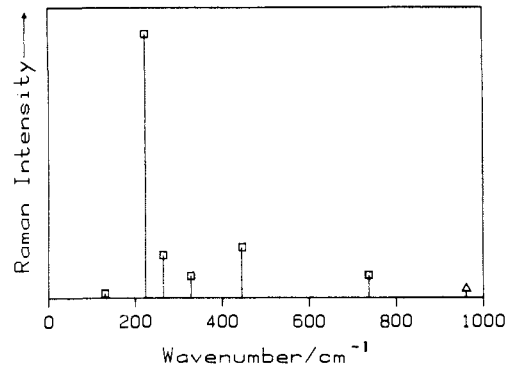

Figure 4. Calculated and experimental (CsCl disc, ca. 80 K) resonance Raman spectrum of $Cs_4[W_2OCl_{10}]$ at 520.8-nm excitation: solid line, experimental intensities; boxes and triangles, calculated intensities.

Table I. Calculated Displacement Δ_k's

complex	ω_k,[a] cm^{-1}	assignment	Δ_k[b]
$Cs_4[W_2OCl_{10}]$[c]	130.0	$\nu_4(\delta(O–W–Cl_{eq}))$	0.90
	223.3	ν_1(W–O–W)	4.00
	264.5	ν_3(W–Cl_{eq})	1.36
	328.0	ν_2(W–Cl_{ax})	0.78
$Cs_3[Re_2OCl_{10}]$[d]	137.1	$\nu_4(\delta(O–Re–Cl_{eq}))$	1.20
	229.8	ν_1(Re–O–Re)	4.00
	288.2	ν_3(Re–Cl_{eq})	0.76
	354.7	ν_2(Re–Cl_{ax})	0.82

[a] At ca. 80 K. [b] The Δ_k's are the displacements of the dimensionless normal coordinates. [c] $E_{00} = 16100 \pm 500$ cm^{-1} (estimated from the electronic absorption spectrum), $\Gamma = 1250$ cm^{-1}, and $\omega_l = 520.8$ nm (19201 cm^{-1}), $\omega_j = 370.7$ cm^{-1} (ν_9), and $\omega_j' = 110$ cm^{-1}. [d] $E_{00} = 17600 \pm 200$ cm^{-1} (estimated from the electronic absorption spectrum), $\Gamma = 140$ cm^{-1}, and $\omega_l = 514.5$ nm (19436 cm^{-1}), $\omega_j = 411.3$ cm^{-1} (ν_9), and $\omega_j' = 190$ cm^{-1}.

The calculated full-width at half-maximum and the peak maximum are 3450 and 18 475 cm^{-1}, respectively. The experimentally observed values are 3275 and 18 100 cm^{-1}, respectively.

The calculated intensities for all of the observed fundamental, overtone, and combination bands at an excitation wavelength of 520.8 nm (19 201 cm^{-1}) are compared with the experimental resonance Raman spectrum in Figure 4. The experimental Raman intensites are represented by vertical solid lines and the calculated intensities by squares or triangles. The numerical values

Table II. Calculated and Observed Intensities of Bands Observed in the Resonance Raman Spectrum of $Cs_4[W_2OCl_{10}]$

calcd intensity[a]	obsd intensity	ω_k, cm^{-1}	assignment
1.7	1.7	130.0	$\nu_4(\delta(O-W-Cl_{eq}))$
100.0	100.0	223.3	$\nu_1(W-O-W)$
16.3	16.1	264.5	$\nu_3(W-Cl_{eq})$
8.3	8.3	328.0	$\nu_2(W-Cl_{ax})$
19.3	19.2	444.6	$2\nu_1$
8.6	8.3	737.4	$2\nu_9$
3.3	2.5	960.1	$\nu_1 + 2\nu_9$

[a] Calculated by using the parameters in Table I, ω_l = 520.8 nm.

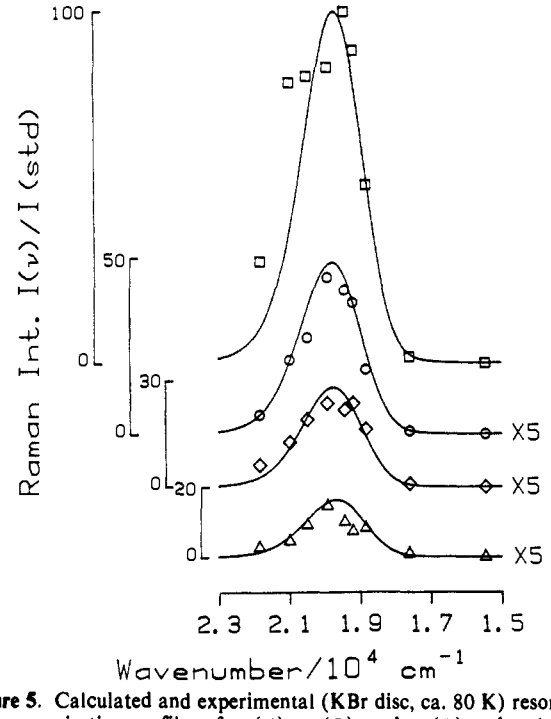

Figure 5. Calculated and experimental (KBr disc, ca. 80 K) resonance Raman excitation profiles of ν_1 (□), ν_2 (○), and ν_3 (◇) and ν_4 (△) for $Cs_3[Re_2OCl_{10}]$.

of the calculated Raman band intensities are compared to the experimental values in Table II. The calculated resonance Raman intensities are in very good agreement with those in the experimental spectrum.

The doubly degenerate non-totally symmetric ν_9 mode (370.7 cm^{-1}) is modelled by using two one-dimensional modes that have the same wavenumber for the ground electronic state and by two inverted harmonic oscillator surfaces for the excited electronic state. A value of 110 cm^{-1} is used for the inverted harmonic oscillator in the calculation. The spreading of the wavepacket on the inverted harmonic surface in the two dimensions effectively quenches the recurrences of the overlap along the totally symmetric modes. This quenching results in smooth excitation profiles in the frequency domain. This aspect of the inverted potential surface is similar to that of the damping factor.

The magnitudes of the displacements of the totally symmetric modes are insensitive to the non-totally symmetric mode. The excitation profiles and the resonance Raman spectrum of the $[W_2OCl_{10}]^{4-}$ ion were calculated without the non-totally symmetric modes and the inverted harmonic oscillator surfaces. The calculation shows the same results as the ones with non-totally symmetric modes.

$Cs_3[Re_2OCl_{10}]$. The excitation profiles of best fit for the fundamentals ν_1(Re–O–Re), ν_2 ($ReCl_{ax}$), ν_3($ReCl_{eq}$), and $\nu_4(\delta_s$-($OReCl_{eq}$)) are shown in Figure 5. They are calculated by use of the parameters given in Table I. The calculated and experimental excitation profiles are in good agreement with one another. The band widths, shapes, and relative intensities of each excitation profile are accurately calculated. All the calculated excitation profiles are normalized to the maximum of the ν_1 band. The maxima of the calculated excitation profiles are at ~19800 cm^{-1}.

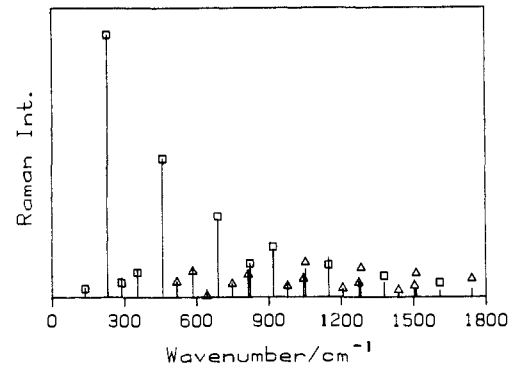

Figure 6. Calculated and experimental resonance Raman spectrum of $Cs_3[Re_2OCl_{10}]$ at 514.5-nm excitation: solid line, experimental intensities; boxes and triangles, calculated intensities.

Table III. Calculated and Observed Intensities of Bands Observed in the Resonance Raman Spectrum of $Cs_3[Re_2OCl_{10}]$

calcd intensity[a]	obsd intensity	ω_k, cm^{-1}	assignment
3.3	3.6	137.1	$\nu_4(\delta(O-Re-Cl_{eq}))$
100.0	100.0	229.8	ν_1(Re–O–Re)
5.5	7.2	288.2	$\nu_3(Re-Cl_{eq})$
9.4	10.8	354.7	$\nu_2(Re-Cl_{ax})$
53.0	53.0	459.2	$2\nu_1$
5.8	6.0	518.3	$\nu_1 + \nu_3$
9.9	11.4	583.9	$\nu_1 + \nu_2$
0.5	3.0	643.6	$\nu_2 + \nu_3$
31.0	29.5	688.9	$3\nu_1$
5.1	5.4	748.4	$2\nu_1 + \nu_3$
8.5	10.2	812.6	$2\nu_1 + \nu_2$
12.8	13.0	822.6	$2\nu_9$
19.2	18.1	918.5	$4\nu_1$
4.2	5.4	977.8	$3\nu_1 + \nu_3$
6.9	8.4	1042.3	$3\nu_1 + \nu_2$
13.2	10.8	1051.4	$\nu_1 + 2\nu_9$
12.3	15.1	1146.5	$5\nu_1$
3.3	3.0	1206.5	$4\nu_1 + \nu_3$
5.5	6.0	1271.5	$4\nu_1 + \nu_2$
11.2	6.0	1279.2	$2\nu_1 + 2\nu_9$
8.1	5.4	1375.8	$6\nu_1$
2.6	1.2	1436.4	$5\nu_1 + \nu_3$
4.3	3.0	1499.6	$5\nu_1 + \nu_2$
9.0	3.0	1507.4	$3\nu_1 + 2\nu_9$
5.4	2.4	1603.4	$7\nu_1$
7.0	3.0	1734.6	$4\nu_1 + 2\nu_9$

[a] Calculated by using the parameters in Table I, ω_l = 514.5 nm, sample at ca. 80 K.

The maximum of the electronic band of interest is at 19900 cm^{-1}.

The absorption spectrum can also be calculated by using the same parameters that were used to calculate the excitation profiles. The calculated full-width at half-maximum and the peak maximum are 1913 and 19850 cm^{-1}, respectively. The experimentally observed values are 2000 and 19900 cm^{-1}, respectively.

The calculated intensities for all of the observed fundamental, overtone, and combination bands at the excitation wavelength 514.5 nm (19436 cm^{-1}) are compared to the experimental resonance Raman spectrum in Figure 6. The Raman intensities in the experimental spectrum are represented by vertical solid lines. The calculated intensities are represented by squares and triangles. The numerical values for the calculated Raman band intensities are compared to the experimental values in Table III. The calculated resonance Raman intensities are in very good agreement with those in the experimental spectrum.

The doubly degenerate non-totally symmetric ν_9 mode (411.3 cm^{-1}) is modelled by using two one-dimensional modes that have the same wavenumber for the ground electronic state and by two inverted harmonic oscillator surfaces for the excited electronic state. A value of 190 cm^{-1} is used for the inverted harmonic oscillator in this calculation.

The principal progression-forming mode, ν_1, is very close to being a simple harmonic oscillator up to vibrational quantum

number 6, with the anharmonicity constant $x_{11} = -0.11$ cm^{-1}. The overtone band wavenumbers derived from the calculation differ from the experimental values by a few cm^{-1} as the vibrational quantum number increases. Other modes show only one harmonic. The assumption used in the calculation that the potential surface are harmonic is reasonable for this molecule.

The damping factor used in the calculation is 140 cm^{-1}. In the absence of the spreading wavepacket on the inverted potential surface, this damping factor would be small enough to give recurrences in the overlap in the time domain. However, the inclusion of the spreading of the wavepacket along the non-totally symmetric mode quenches the recurrences to give smooth excitation profiles.

The magnitudes of the displacements of the totally symmetric modes are insensitive to the non-totally symmetric mode. The excitation profiles and the resonance Raman spectrum of the $[Re_2OCl_{10}]^{3-}$ ion were calculated without the non-totally symmetric mode and the inverted harmonic oscillator surfaces. This calculation gave the same results as the one with non-totally symmetric modes. In this case, a higher damping factor (200 cm^{-1} instead of 140 cm^{-1}) was used to get the smooth excitation profiles.

Quantitative Evaluation of Bond Length and Bond Angle Changes on Excitation. The relationship between the changes in normal coordinates (ΔQ's) and the changes in symmetry coordinates (ΔS's) for $[Re_2OCl_{10}]^{3-}$ was studied by Campbell and Clark.[19] The relationship between the ΔQ's and ΔS's is

$$\begin{pmatrix} \Delta Q_1 \\ \Delta Q_2 \\ \Delta Q_3 \\ \Delta Q_4 \end{pmatrix} = \begin{pmatrix} 0.46 & 0.28 & 0.00 & 0.25 \\ 0.22 & 0.63 & 0.00 & 0.15 \\ 0.00 & 0.01 & 0.99 & 0.00 \\ 0.27 & 0.13 & 0.00 & 0.60 \end{pmatrix} \begin{pmatrix} \Delta S_1 \\ \Delta S_2 \\ \Delta S_3 \\ \Delta S_4 \end{pmatrix} \quad (6)$$

The symmetry coordinates are

$$\Delta S_1 = (1/\sqrt{2})\sum \Delta r(\mathrm{ReO}) \quad (7)$$

$$\Delta S_2 = (1/\sqrt{2})\sum \Delta r(\mathrm{ReCl_{ax}}) \quad (8)$$

$$\Delta S_3 = (1/\sqrt{8})\sum \Delta r(\mathrm{ReCl_{eq}}) \quad (9)$$

$$\Delta S_4 = (1/4)[\sum \Delta\beta - \sum \Delta\alpha] \quad (10)$$

where $\beta = \angle \mathrm{Cl_{ax}ReCl_{eq}}$ and $\alpha = \angle \mathrm{OReCl_{eq}}$.

The individual bond length and bond angle changes are calculated by using eq 6–10. For example, the Re–O bond length change is calculated in the following manner. By rearranging eq 6,

$$\Delta S_1 = 0.46\Delta Q_1 + 0.22\Delta Q_2 + 0.27\Delta Q_4 \quad (11)$$

Inserting the ΔQ's from Table I gives $\Delta S_1 = 2.34$. From eq 7, $\Delta r(\mathrm{Re–O}) = (1/\sqrt{2})\Delta S_1 = 1.65$. To convert from the dimensionless normal coordinates used in the time-dependent calculation to angstroms, the relative atomic mass of the Re atom is used.[23] The individual Re–O bond length change in $[Re_2OCl_{10}]^{3-}$ is 0.046 Å. Since only the magnitudes of ΔQ's are determined from the calculation (not the sign), it is assumed that the signs of the changes of all ΔQ's are the same in the $e_u(\pi^*)$ orbital. The Re–O bond length change will be smaller if the signs of the changes in ΔQ's are different from one another.

The maximum $\mathrm{Re–Cl_{ax}}$ bond length change is 0.026 Å. It is calculated by using the same procedure as that described above. The relative atomic mass used to convert dimensionless Δ into angstrom units for ΔS_2 (1.8) is the sum of the masses of rhenium and chlorine.

(23) The formula to convert the dimensionless displacement Δ into Å is

$$\delta = \sqrt{\frac{6.023 \times 10^{23}}{m} \frac{\hbar}{2\pi c\omega}} \times 10^8 \times \Delta$$

where m is the mass involved in the vibration in the units of gram atomic weight (e.g. $C = 12$ g), ω is the wavenumber of the vibrational mode in cm^{-1}, $\hbar = h/2\pi$ where h is Planck's constant in g cm^2 s^{-1}, c is the speed of light in cm s^{-1}, δ is the displacement in Å, and Δ is the dimensionless displacement.

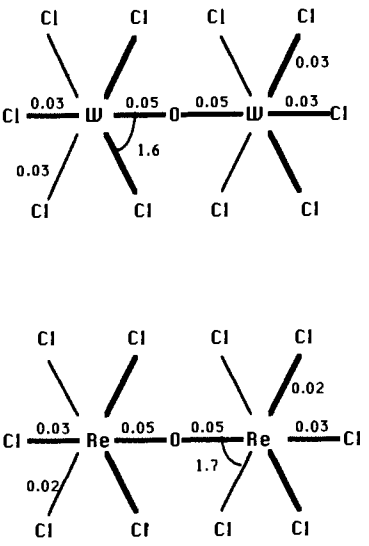

Figure 7. The calculated changes in bond lengths and angles for $[Re_2OCl_{10}]^{3-}$ and $[W_2OCl_{10}]^{4-}$ ions.

The $\mathrm{Re–Cl_{eq}}$ bond length change of the $[Re_2OCl_{10}]^{3-}$ ion is 0.016 Å. The mass used to convert the dimensionless Δ into angstrom units for ΔS_3 (0.76) is the mass of chlorine.

The $\mathrm{O–Re–Cl_{eq}}$ bond angle change of the $[Re_2OCl_{10}]^{3-}$ ion is 1.7°. It is also calculated by using the same procedure as described above. The mass used to convert the dimensionless ΔS_4 (1.84) into degrees is $1/(2\mu_{Cl} + 8\mu_{Re})\rho^2$, where μ_{Cl} is the reduced mass of chlorine, μ_{Re} is the reduced mass of rhenium, and ρ^2 is $1/r(\mathrm{ReCl_{eq}})^2$.

The structural changes in the case of the $[W_2OCl_{10}]^{4-}$ ion on excitation to the resonant state have been calculated by using the same method as that used for the $[Re_2OCl_{10}]^{3-}$ ion. Since no force field analysis has been done on the $[W_2OCl_{10}]^{4-}$ ion, the potential energy distribution of the normal coordinates used for $[Re_2OCl_{10}]^{3-}$ was also used for the $[W_2OCl_{10}]^{4-}$ ion to calculate its bond length and bond angle changes. The results are that the W–O, $\mathrm{W–Cl_{ax}}$, and $\mathrm{W–Cl_{eq}}$ bond lengths change by 0.046, 0.027, and 0.029 Å, respectively. The $\mathrm{O–W–Cl_{eq}}$ bond angle changes by 1.58°.

Interpretation of the Bond Length and Angle Changes. The calculated changes in bond lengths (in Å) and angles (in deg) for $[Re_2OCl_{10}]^{3-}$ ion and $[W_2OCl_{10}]^{4-}$ are shown in Figure 7. The principal structural changes are in the axial direction. This is fully consistent with the idea that the resonant transition is the axially polarized, electric-dipole allowed transition of the π-bonded system. In orbital terms, this transition involves excitation of an electron from a nonbonding $e_g(\pi)$ orbital to an antibonding $e_u(\pi^*)$ orbital and, as such, would be expected to lead to an increase in the M–O bond lengths and to changes in the $\mathrm{M–Cl_{ax}}$ bond lengths on account of their extensive coupling to $\nu(\mathrm{M–O–M})$. A schematic representation of the axial e_g and e_u π-molecular orbitals of the $[M_2OX_{10}]^{n-}$ ions is shown below.

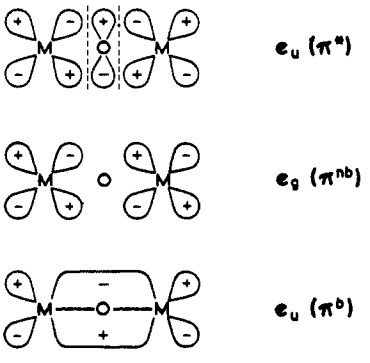

The magnitudes of the bond length and angle changes are very similar in the $[Re_2OCl_{10}]^{3-}$ and $[W_2OCl_{10}]^{4-}$ ions. The small differences will not be interpreted because the potential energy distribution of the normal coordinates for $[W_2OCl_{10}]^{4-}$ is lacking.

The magnitudes of the bond length changes are comparable with those (~0.03 Å) calculated by Frank-Condon analyses[24] to take place in $[MnO_4]^-$,[24,25] $[MnO_4]^{2-}$,[7] $[MoS_4]^{2-}$,[8] and $[WS_4]^{2-}$,[9] on exciting the highest nonbonding electron to the lowest antibonding orbital.

Acknowledgment. This work is made possible by Grant NSF CHE 88-06775 from the National Science Foundation (K.S.S., J.I.Z.). J.I.Z. also gratefully acknowledges a fellowship from the John Simon Guggenheim Memorial Foundation, which was held in part at University College London.

(24) Clark, R. J. H.; Dines, T. J. *Angew. Chem., Int. Ed.* **1986**, *25*, 131.
(25) Clark, R. J. H.; Stewart, B. *J. Am. Chem. Soc.* **1981**, *103*, 6593.

Electronic Absorption and MCD Spectra of $M_2(TMB)_4^{2+}$, M = Rh and Ir. A Valence-Bond Description of the Upper Electronic Excited States

David C. Smith,† Vincent M. Miskowski,† W. Roy Mason,‡ and Harry B. Gray*,†

Contribution No. 7970 from the Arthur Amos Noyes Laboratory, California Institute of Technology, Pasadena, California 91125, and Department of Chemistry, Northern Illinois University, DeKalb, Illinois 60115. *Received August 7, 1989*

Abstract: Electronic absorption and magnetic circular dichroism (MCD) spectra of $Rh_2(TMB)_4^{2+}$ and $Ir_2(TMB)_4^{2+}$ are reported along with polarized single-crystal absorption spectra of $[Ir_2(TMB)_4][B(C_6H_5)_4]_2 \cdot CH_3C_6H_5$ (TMB = 2,5-diisocyano-2,5-dimethylhexane). Interpretation of the spectra is based on a valence-bond model that accommodates highly perturbed dimer transitions as well as monomer-like dimer excitations. In this model, half of the dimer electronic excited states possess ionic character; these states involve metal-to-metal charge transfer (MMCT). The intense absorptions of $Ir_2(TMB)_4^{2+}$ are assigned as follows: $d\sigma^* \rightarrow p\sigma$ [$A_{1g}(^1A_{1g}) \rightarrow E_u(^3A_{2u})$ and $A_{2u}(^1A_{2u})$] at 820 and 635 nm; $d_{xz,yz} \rightarrow p_z$ [$A_{1g}(^1A_{1g}) \rightarrow E_u$, $A_{2u}(^3E_u)$ and $E_u(^1E_u)$] at 373, 331, and 320 nm; and $d_{xy} \rightarrow p_z$ [$A_{1g}(^1A_{1g}) \rightarrow E_u(^3B_{1u})$] at 304 nm. Several weak features are observed to lower energy of the $A_{1g}(^1A_{1g}) \rightarrow E_u(^3A_{2u})$ band. The most prominent of the weak features (~430 nm) is assigned to the transition to $^1A_{1g}$ (a single-center $d_{z^2} \rightarrow p_z$ excitation). High-energy features ($\lambda < 300$ nm) in the spectra of $Rh_2(TMB)_4^{2+}$ and $Ir_2(TMB)_4^{2+}$ are assigned to MMCT arising from $d_{xz,yz} \rightarrow p_z$ excitations.

The electronic spectra of face-to-face, metal-metal-bonded d^8-d^8 complexes have been extensively discussed on the basis of a molecular orbital (MO) model.[1-10] In this picture, the metal-based d_{z^2} (filled) and p_z (empty) orbitals each interact strongly to produce pairs of bonding and antibonding orbitals. Configuration interaction between the empty and filled sets (which might alternatively be visualized as dative d-p bonding) provides the weak ground-state bond, while the lowest energy singlet and triplet excited states, derived from the $d\sigma^* \rightarrow p\sigma$ one-electron transition, are strongly stabilized relative to their respective monomer $d_{z^2} \rightarrow p_z$ states.

While this picture accounts for some important aspects of the metal-metal interaction, it also has been noted that several monomer d → p excitations are only slightly perturbed in the d^8-d^8 complexes.[1] This observation and the rather long metal-metal bonds (3.1-3.3 Å)[11,12] suggest that d^8-d^8 species should be examined in terms of valence-bond (VB) theory.

In addition to beginning such an examination, and to complement earlier investigations of rhodium complexes ($Rh_2(TMB)_4^{2+}$, TMB = 2,5-diisocyano-2,5-dimethylhexane; $Rh_2b_4^{2+}$, b = 1,3-diisocyanopropane), we undertook a detailed study of the electronic spectrum of $Ir_2(TMB)_4^{2+}$. A change in the metal from rhodium to iridium should perturb the electronic structure, thereby altering the characteristic d^8-d^8 electronic spectrum and allowing us to test key aspects of the MO and VB models. We report here the electronic absorption and magnetic circular dichroism (MCD) spectra of $Rh_2(TMB)_4^{2+}$ and $Ir_2(TMB)_4^{2+}$ along with polarized single-crystal absorption spectra of $[Ir_2(TMB)_4][B(C_6H_5)_4]_2 \cdot CH_3C_6H_5$.

Experimental Section

All synthetic procedures were carried out with standard Schlenk techniques unless otherwise specified. Tetrahydrofuran (THF) was distilled from CaH_2 prior to use. Other solvents were taken from freshly opened bottles and were not purified further, except as noted. All solvents were Schlenk degassed prior to use. Standard procedures were used to prepare 2,5-diisocyano-2,5-dimethylhexane (TMB),[11] $[Ir_2(TMB)_4][B(C_6H_5)_4]_2$,[13] $[Ir(COD)Cl]_2$ (COD = 1,5-cyclooctadiene),[14] $[Ir(COD)_2]BF_4$,[15] and $[Rh_2(TMB)_4](PF_6)_2$.[11] The literature preparation of Ir(COD)(acac) (acac = acetylacetone),[16] a precursor to $[Ir(COD)_2]BF_4$, was modified as noted below. All other chemicals were reagent grade or comparable quality and were used as received. The ^1H NMR spectra were obtained on a 400-MHz JNM-GX400 FT NMR spectrometer.

* To whom correspondence should be addressed.
† California Institute of Technology.
‡ Northern Illinois University.

(1) Rice, S. F.; Miskowski, V. M.; Gray, H. B. *Inorg. Chem.* **1988**, *27*, 4704-4708.
(2) Stiegman, A. E.; Rice, S. F.; Gray, H. B.; Miskowski, V. M. *Inorg. Chem.* **1987**, *26*, 1112-1116.
(3) Isci, H.; Mason, W. R. *Inorg. Chem.* **1985**, *24*, 1761-1765.
(4) Rodman, G. S.; Daves, C. A.; Mann, K. R. *Inorg. Chem.* **1988**, *27*, 3347-3353.
(5) Milder, S. J.; Kliger, D. S. *J. Phys. Chem.* **1985**, *89*, 4170-4171.
(6) Milder, S. J. *Inorg. Chem.* **1984**, *24*, 3376-3378.
(7) Milder, S. J.; Kliger, D. S.; Butler, L. G.; Gray, H. B. *J. Phys. Chem.* **1986**, *90*, 5567-5570.
(8) Winkler, J. R.; Marshall, J. L.; Netzel, T. L.; Gray, H. B. *J. Am. Chem. Soc.* **1986**, *108*, 2263-2266.
(9) Marshall, J. L.; Stiegman, A. E.; Gray, H. B. in *Excited States and Reactive Intermediates*; Lever, A. B. P., Ed.; ACS Symposium Series 307; American Chemical Society: Washington, DC, 1986; pp 166-176.
(10) Mann, K. R.; Gordon, J. G., II.; Gray, H. B. *J. Am. Chem. Soc.* **1975**, *97*, 3553-3555.
(11) Mann, K. R.; Thich, J. A.; Bell, R. A.; Coyle, C. L.; Gray, H. B. *Inorg. Chem.* **1980**, *19*, 2462-2468.
(12) Smith, D. C. Ph.D. Thesis, California Institute of Technology, 1989.
(13) Miskowski, V. M.; Smith, T. P.; Loehr, T. M.; Gray, H. B. *J. Am. Chem. Soc.* **1985**, *107*, 7925-7934.
(14) Herde, J. L.; Lambert, J. C.; Senoff, C. V. *Inorg. Synth.* **1974**, *15*, 18-20.
(15) Green, M.; Kuck, T. A.; Taylor, S. H. *J. Chem. Soc. A* **1971**, 2334-2337.
(16) Robinson, S. D.; Shaw, B. L. *J. Chem. Soc.* **1965**, 4997-5001.

0002-7863/90/1512-3759$02.50/0